

Effects of Structural Disorder and Surface Chemistry on Electric Conductivity and Capacitance of Porous Carbon Electrodes

⁵ Boris Dyatkin^a and Yury Gogotsi^{a*}
DOI: 10.1039/b000000x [DO NOT ALTER/DELETE THIS TEXT]

Supporting Information

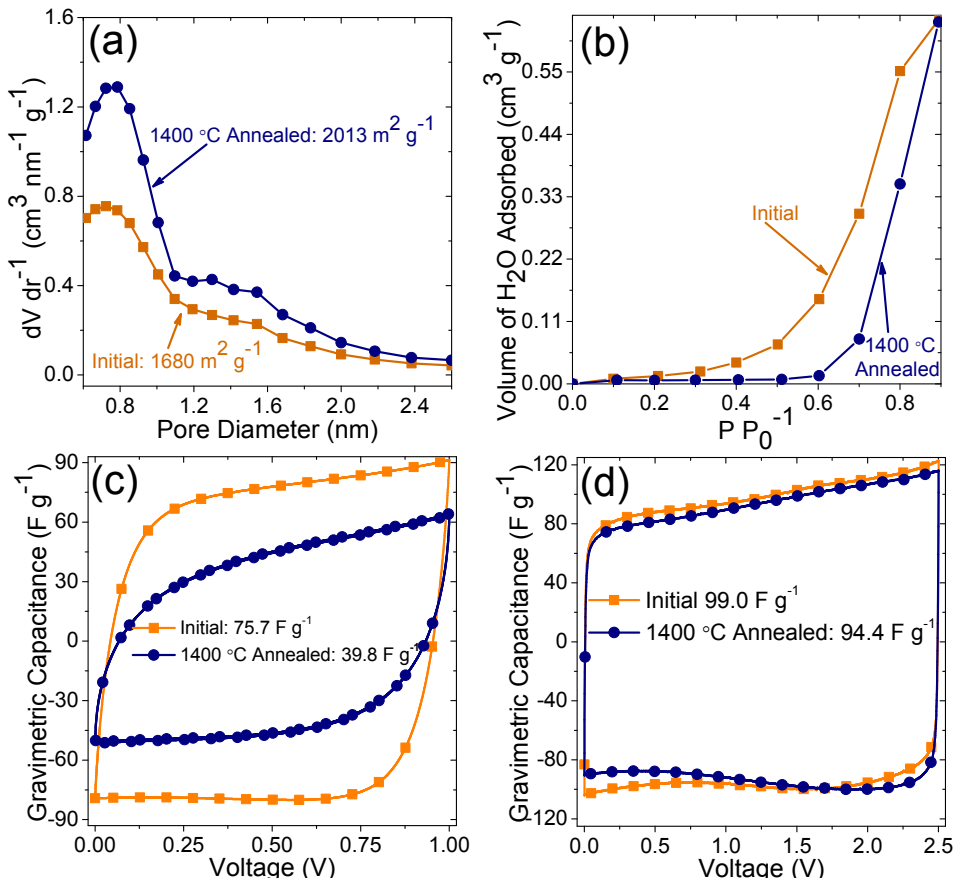


Fig S1. (a) Pore size distributions and BET-derived specific surface area of TiC-CDC microparticles that were synthesized at $1000 \text{ }^\circ\text{C}$ and annealed at $1400 \text{ }^\circ\text{C}$. Initial high degree of ordering minimizes pore collapse and expands pore volume through defunctionalization and some additional graphitization. (b) Dynamic water vapour sorption of the initial and annealed materials, indicating similar increase in hydrophobicity as observed for the $800 \text{ }^\circ\text{C}$ synthesized systems. (c) Performance of the materials in $1.0 \text{ M Na}_2\text{SO}_4$ aqueous electrolyte, indicating a significant decrease in capacitance and a large resistance increase for the annealed material due to poor pore wetting. (d) Electrochemical performance of these materials in a (more hydrophobic) electrolyte of $1.0 \text{ M NEt}_4\text{-BF}_4$ in acetonitrile, exhibiting similar ionic resistance, fewer faradic reactions, and no increases in capacitance of the $1400 \text{ }^\circ\text{C}$ annealed material despite higher SSA and increased material conductivity.

15

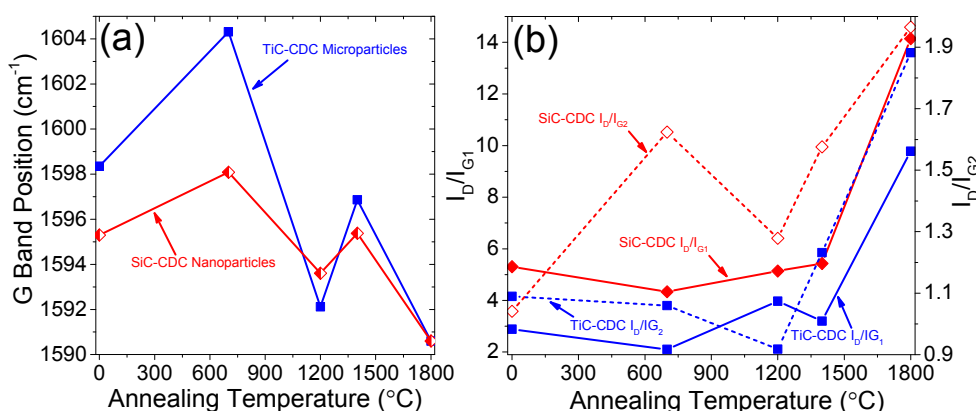
^a A.J. Drexel Nanomaterials Institute & Department of Materials Science and Engineering, 3141 Chestnut Street, Philadelphia, PA 19104, USA. Fax: 2158951934; Tel: 2158956446; E-mail: gogotsi@drexel.edu

[journal], [year], [vol], 00–00 | 1

This journal is © The Royal Society of Chemistry [year]

Table S1. Surface area, pore volume, and pore size distribution values derived from N₂ gas sorption for the microparticles and nanoparticles in their initial and annealed states.

	TiC-CDC Microparticles			SiC-CDC Nanoparticles		
	Initial CDC	700 °C Annealed	1400 °C Annealed	Initial CDC	700 °C Annealed	1400 °C Annealed
BET SSA, m ² g ⁻¹	1682	1946	1371	2001	3101	1401
DFT SSA, m ² g ⁻¹	1699	1870	1337	1762	2899	1290 ¹
Cumulative pore volume, cm ³ g ⁻¹	0.65	0.77	0.58 ¹	1.44	2.04	1.21
Subnanometer pore volume, cm ³ g ⁻¹	0.48 ¹	0.53	0.36	0.42	0.77	0.30
Pore diameter mode, nm	0.61	0.67	0.67	0.85	1.01	0.79

**Fig S2.** (a) Position of the G band and effects of annealing on its shifts. (b) Ratios of normalized intensities of the D band to two components of the G band: G1 (1550 cm⁻¹) accounting for amorphous sp² phase contributions⁵ and G2 (1595 cm⁻¹) accounting for ordered sp² graphitic domains.¹

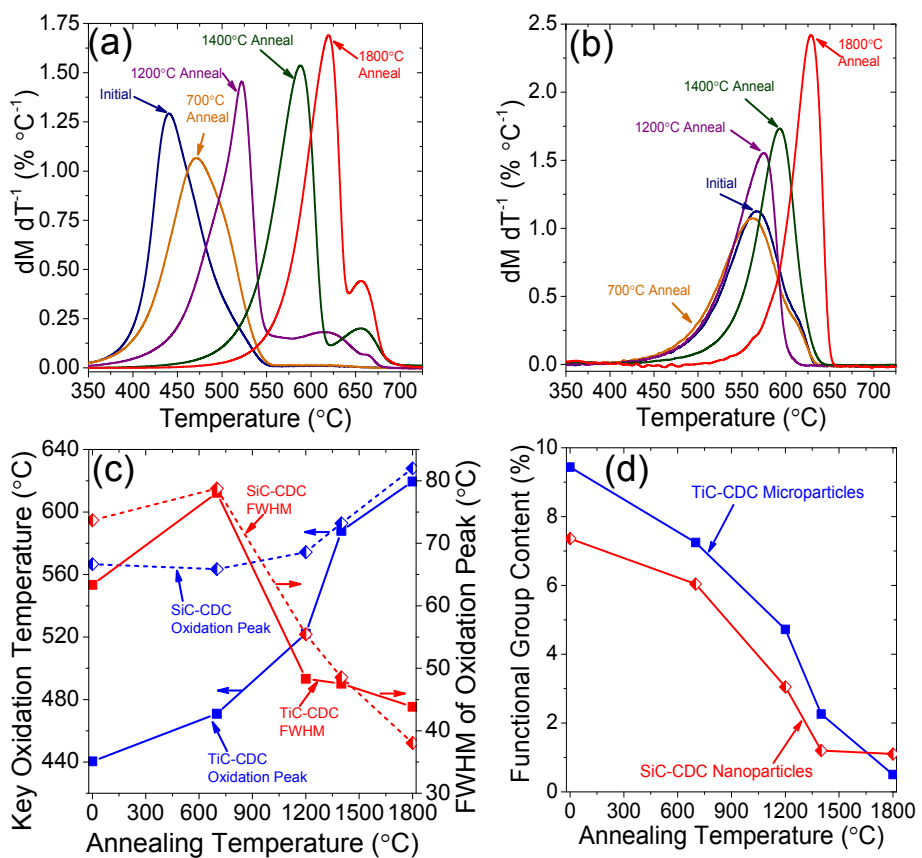


Fig S3. Oxidation peaks determined using TGA in air environment for (a) microparticles and (b) nanoparticles. (c) These peaks show a shift to higher oxidation temperatures and a more narrow distribution as annealing temperature increases, suggesting that the material becomes more ordered and homogeneous. (d) Percentage of mass lost during heating of samples to 800 °C (TGA in an Ar environment), corresponding to amounts of non-carbon functional groups that undergo decomposition.²

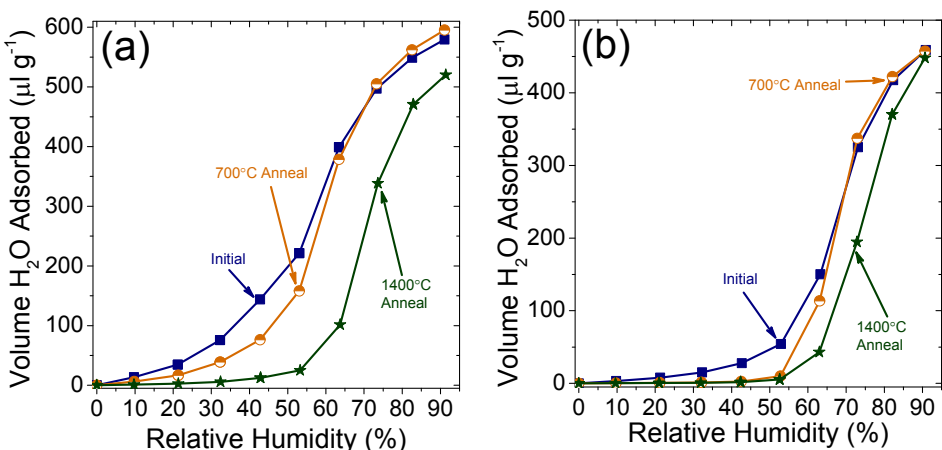
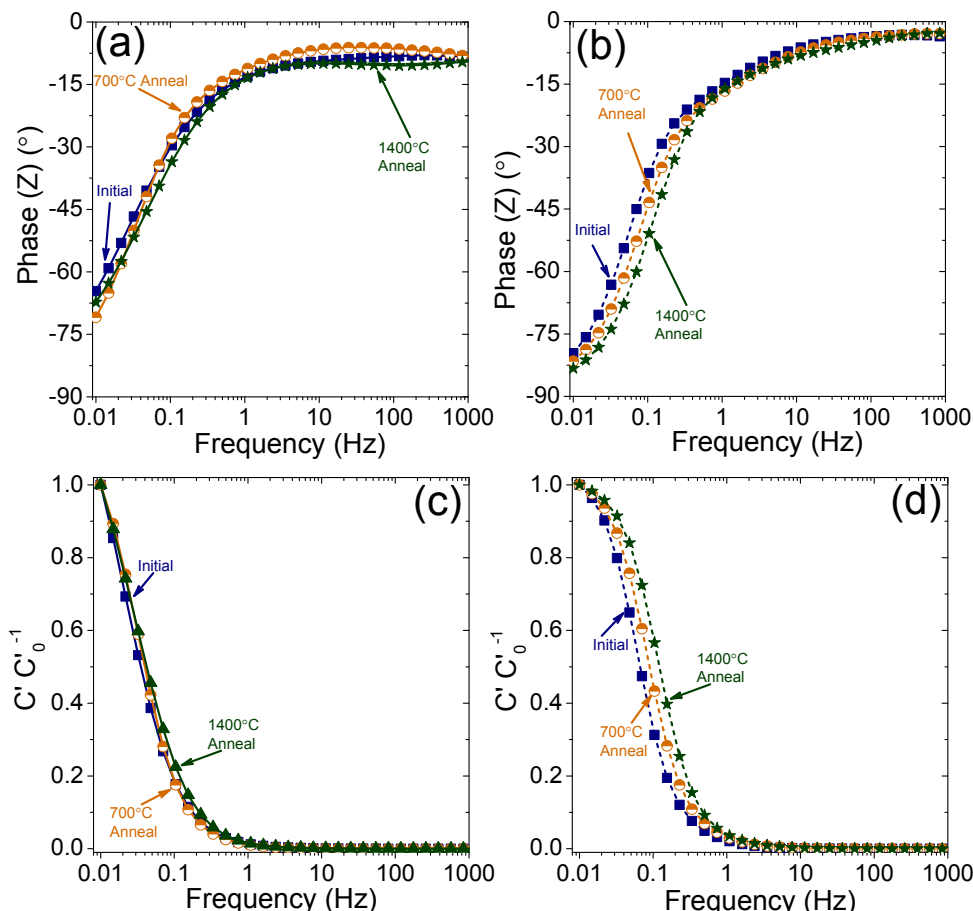


Fig S4. Dynamic water vapour sorption on (a) TiC-CDC microparticles and (b) SiC-CDC nanoparticles. Water adsorption was carried out at 25 °C isotherms using an 80 min equilibration stage for each relative humidity step.⁵

Table S2. Distributions of charge storage and capacitance from the working (WE) and counter (CE) electrodes, as collected from the various systems at 5 mV s⁻¹ in a 0.0 – 2.5 V window.

	TiC-CDC Microparticles			SiC-CDC Nanoparticles		
	Initial CDC	700 °C Annealed	1400 °C Annealed	Initial CDC	700 °C Annealed	1400 °C Annealed
WE – Stored charge, %	79.2	79.2	58.6	67.6	71.5	47.6
CE – Stored charge, %	20.8	20.8	41.4	32.4	28.4	52.4
WE – Capacitance, %	49.5	53.0	51.1	45.4	48.1	50.6
CE – Capacitance, %	50.5	47.0	48.9	54.6	51.9	49.4

5

**Fig S5.** Phase angle plots highlighting response of impedance to voltage oscillation frequency for (a) microparticles and (b) nanoparticles. A phase angle of -90° signifies double layer capacitance as the sole contributor to impedance. Bode impedance plots for (c) microparticles and (d) nanoparticles normalized by the real capacitance measured at 10 mHz.

10

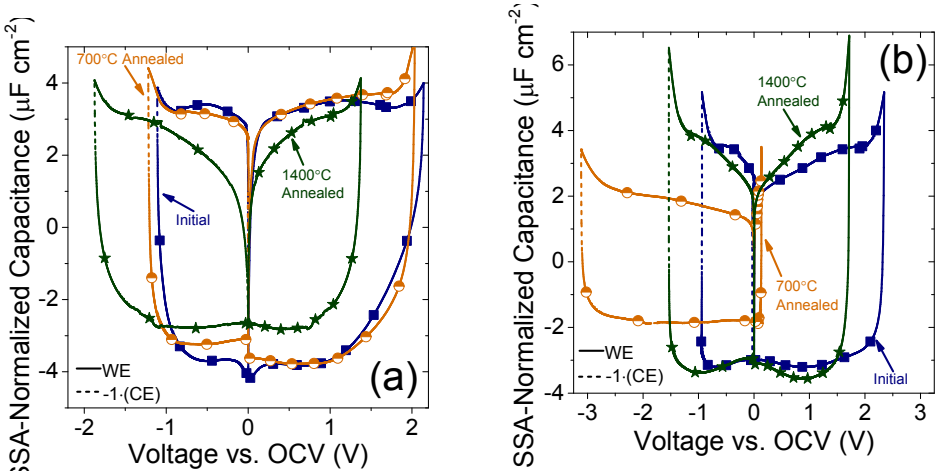


Fig S6. Performances of working and counter electrodes in a 3.25 V operating window measured using cyclic voltammetry conducted at 2 mV s^{-1} for (a) microparticles and (b) nanoparticles. Data shown is the first cycle of this potential window. Voltammograms are plotted vs. open circuit voltage (OCV). The values for the initial, 700 °C annealed, and 1400 °C annealed samples were, respectively, -57.5 mV, -498.7 mV, and -16.8 mV for microparticles and -356.0 mV, 22.1 mV, and -120.9 mV for nanoparticles. As in Fig. 6, the negative current is plotted for the working electrode for each material, in order to facilitate symmetry comparison. Previously, each system was cycled multiple times in the 0.0 – 2.5 V window, and cycled twice to 2.75 V and 3.00 V. Narrowing of specific electrodes (such as the WE of the 700 °C annealed nanoparticle sample) is possibly attributed to selective decomposition of one ion (in this case, the TFSI⁻ ion in the working electrode) and its relative

10

Table S3. Coulombic efficiencies of working and counter electrodes, as collected from the various systems (shown in Fig. S6) at 2 mV s^{-1} in a 0.0 – 3.25 V window.

	TiC-CDC Microparticles			SiC-CDC Nanoparticles		
	Initial CDC	700 °C Annealed	1400 °C Annealed	Initial CDC	700 °C Annealed	1400 °C Annealed
WE – Coulombic Efficiency, %	86.6	88.9	86.2	93.1	94.9	89.1
CE – Coulombic Efficiency, %	96.6	92.4	97.1	58.7	95.1	91.9

15

20

25

30

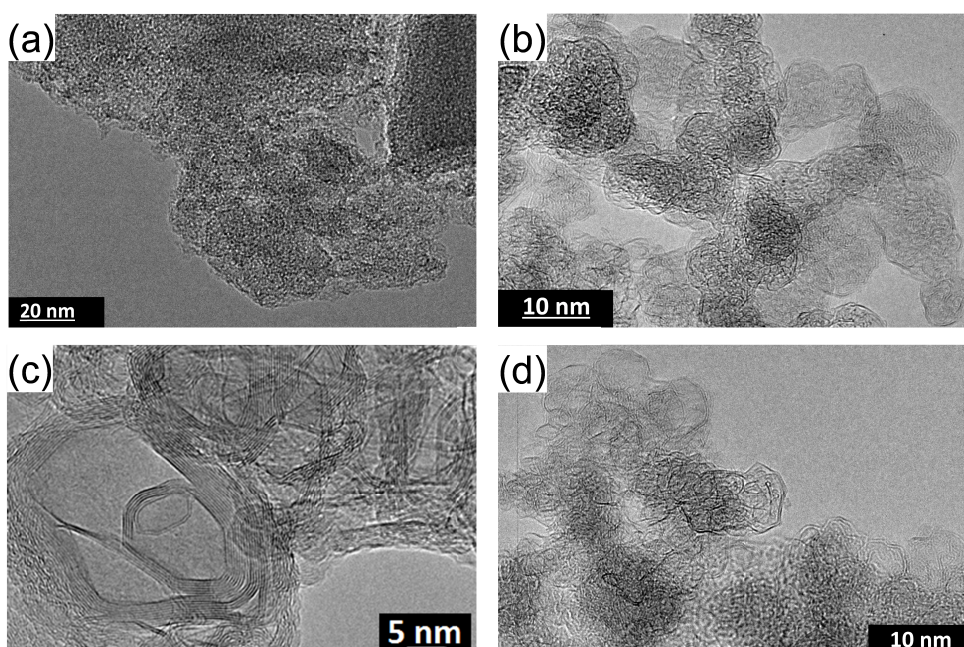


Fig S7. TEM micrographs showing the key morphological features that become more prominent as a result of vacuum annealing at high temperatures. For the TiC-CDC microparticles shown in (a), annealing at 1400 °C produces a variety of graphitic ribbons and barrels shown in (c), an increase in turbostratic graphite, and edges terminated with ordered, smooth graphite sheets. SiC-CDC nanoparticles shown in (b) develop mostly graphitic ribbons shown in (d); annealing process is not shown to affect particle size.

Quantum Capacitance Discussion: First Principles Calculations

As detailed in previous fundamental investigations,^{3, 4} the total capacitance of a supercapacitor (modeled as a single sheet of graphene) is properly modeled as 2 capacitors in series as follows:

$$\frac{1}{C_{\text{total}}} = \frac{1}{C_{\text{quantum}}} + \frac{1}{C_{\text{double layer}}} \quad (\text{S1})$$

This relationship therefore states that the smallest capacitor in series has the greatest impact on total capacitance. When considering several stacked graphene sheets, this indicates that the quantum capacitance contribution (governed by electron density of states, E_F level, and Brilloin zone boundaries^{3, 5, 6}) dominates until sheet stacking number reaches 4. When those conditions are exceeded, capacitance from the Stern double layer of electrosorbed ions dominates.⁷

Previous modeling work showed that, for a single, defect-free sheet of graphene, the Dirac point is at 0.0 V and corresponds to a thermally-governed value of 0.8 $\mu\text{F cm}^{-2}$. The capacitance increases nearly linearly from that position in the positive and negative applied voltage directions,³ at an approximate rate of 23 $\mu\text{F cm}^{-2} \text{V}^{-1}$. Although even the materials annealed at 1400 °C have a number of defects that dope the C_{quantum} value (Stone-Wales defects, monovacancies, curvature, some chemical species, etc.), they represent structures that most resembled single graphene sheet, and for a first-principles estimate could be assumed to operate under the linear C_{quantum} vs. voltage (V) relationship.

References

1. J. Chmiola, S. Osswald and Y. Gogotsi, *Carbon*, 2012, **50**, 4880-4886.
2. T. G. Ros, A. J. v. Dillen, J. W. Geus and D. C. Koningsberger, *Chemistry - A European Journal*, 2002, **8**, 1151–1162.
3. J. Xia, F. Chen, J. Li and N. Tao, *Nature Nanotechnology*, 2009, **4**, 505-509.
4. B. C. Wood, T. Ogitsu, M. Otani and J. Biener, *The Journal of Physical Chemistry C*, 2013, **118**, 4-15.
5. H. Ji, X. Zhao, et al. *Nature Communications*, 2014, **5**, 3317.
6. T. Fang, A. Konar, H. Xing and D. Jena, *Applied Physics Letters*, 2007, **91**, 092109.
7. E. Uesugi, H. Goto, R. Eguchi, A. Fujiwara and Y. Kubozono, *Sci. Rep.*, 2013, **3**, 1595.